V. BUBBLE SIZE DISTRIBUTIONS

The overall mass transfer rate per unit volume of the dispersion in a bubble column is governed by the liquid–side mass transfer coefficient ($k_\ell a$), assuming that the gas–side resistance is negligible. In a bubble column reactor, the variation in $k_\ell a$ is primarily due to variations in the interfacial area (Fan, 1989). Assuming spherical bubbles, the specific gas–liquid interfacial area is related to the gas holdup, ϵ_g and the Sauter mean bubble diameter, d_s, by

$$a_s = \frac{6\epsilon_g}{d_s} \tag{5.1}$$

Thus, a precise knowledge of the gas holdup and bubble size distribution is needed to determine the specific gas–liquid interfacial area.

Extensive work on bubble size measurements in two–phase systems has been reported in the literature, and has been reviewed by several authors (e.g. Buchholz and Schugerl, 1979; Shah et al., 1982; Saxena et al., 1988); however, the majority of these studies pertain to air–water systems. Bubble size measurements with molten wax as the liquid medium are rather limited (e.g. Calderbank et al., 1963; Quicker and Deckwer, 1981; O'Dowd et al., 1987; Bukur et al., 1987a,c; Patel et al., 1990) and there is some disagreement between bubble size data reported in these studies. The general consensus is that some molten wax systems depict an unique behavior, namely, an abundance of very small bubbles is present and high gas holdups are obtained in comparison to pure hydrocarbons having similar physical properties. The resulting specific gas–liquid interfacial areas could be an order of magnitude greater than those of pure hydrocarbons (Quicker and Deckwer, 1981). The findings from bubble size measurement studies with molten waxes are summarized below.

Calderbank et al. (1963) used a light transmission technique to measure interfacial areas of Krupp wax at 265 °C for gas velocities less than 0.06 m/s in a 0.05 m ID column equipped with a ball and cone type sparger. When these data, together with the average gas holdup values reported by them, are used in Eq. 5.1, Sauter mean bubble diameters in the range 2 – 3 mm are obtained. Zaidi et al. (1979) and Deckwer et al. (1980) reported a much lower d_s value, 0.7 mm, for paraffin wax using photography in 0.041 and 0.1 m ID columns equipped with 75 μm porous plate spargers (T = 250 – 270 °C, $u_g \leq 0.03$ m / s). Quicker and Deckwer (1981) measured d_s values for FT–300 wax in a 0.095 m ID column equipped with a 0.9 mm nozzle. Sauter mean bubble diameters, determined by the photographic method, at 170 °C ranged from 1.3 mm (u_g = 0.01 m/s) to 0.6 mm (u_g = 0.035 m/s). More recently, O'Dowd et al. (1987) obtained d_s values for a P–22 wax, and for reactor wax from run 7 in Mobil's pilot plant slurry reactor (Unit CT–256) using the hot wire anemometer technique at 250 °C and 1.48 MPa. Their d_s values, from a 0.022 m ID column equipped with a 1 mm orifice plate, for the two waxes were in the range 2.7 to 3.9 mm for $u_g \leq 0.02$ m/s, and are comparable to values reported by Calderbank et al. (1963).

The lower d_s values from the studies conducted by Zaidi et al., Deckwer et al., and Quicker and Deckwer, cannot be attributed to the limitation of the photographic technique (i.e. its bias towards small bubbles in the vicinity of the wall). This is because all of these studies were conducted in the homogeneous bubbling regime ($u_g \leq 0.035$ m/s) where the dispersion is expected to be radially uniform. Discrepancies in results might be due to use of different waxes in these studies. We have shown in our laboratory (Bukur et al., 1987a,c) that hydrodynamic parameters obtained in experiments with different waxes could differ significantly, despite similarites in physical properties of different waxes.

Numerous techniques have been used to measure bubble size distributions. Some of the techniques which are commonly employed are photography, hot wire anemometry, electrical conductivity, and light transmission. More recently, the dynamic gas disengagement (DGD) technique, originally developed by Sriram and Mann, 1977, has been employed (e.g. Vermeer and Krishna, 1981; Kuo, 1985; Bukur et al., 1987a,c; Patel et al., 1989). This technique was used in the present study.

The approach presented by Sriram and Mann has been used by several researchers to determine the holdup structure of the dispersion. In most cases, the dispersion was assumed to consist of one or two dominant bubble sizes. Vermeer and Krishna (1981) applied this approach to the nitrogen–turpentine 5 system. They assumed a bimodal distribution with large bubbles forming the transport portion of the holdup and small, slow rising, bubbles forming the entrained portion. Based on this assumption, they considered the initial part of the disengagement profile to be dictated solely by the large bubbles, with the small bubbles disengaging only after all of the large bubbles have left the system. They used the resulting disengagement profiles to estimate the contribution to the gas holdup by the two bubble classes. Schumpe and Deckwer (1982), and Godbole et al. (1982, 1984) conducted experiments with highly coalescing CMC (carboxymethyl cellulose) systems and used bimodal bubble size distributions to determine the holdup structure of the dispersion by dynamic gas disengagement. For such systems, they showed that the contribution of small bubbles to the overall gas holdup is negligible. In similar experiments with different concentrations of surfactants added to the CMC solution, Godbole et al. (1984) showed that the contribution of small bubbles to the overall gas holdup increased with increasing surfactant concentration (i.e. decreasing coalescence rates), while the contribution due to large bubbles remained virtually unchanged. In experiments conducted with alcohol solutions (noncoalescing media) by Kelkar et al. (1983), similar results were obtained when the holdup structure

was determined using the dynamic gas disengagement technique assuming a bimodal bubble size distribution. For these solutions, the contribution to overall gas holdup by small bubbles was even greater than that due to large bubbles.

More recently, Schumpe and Grund (1986) have presented results for the air–water system, with an emphasis on some of the problems associated with the DGD technique and have proposed corrective measures which to some extent can alleviate these problems. The problems analyzed by the authors include the subjectivity involved in obtaining an accurate disengagement profile during large bubble disengagement, the "waterfall" effect or downward flow of liquid during bubble disengagement and its impact on the rise velocity of small bubbles, and errors introduced by bubbles entering the dispersion as the pressure in the plenum chamber equilibrates with the hydrostatic pressure of the dispersion, following the interruption of the gas supply. The authors assumed a bimodal bubble size distribution in their analysis and presented the gas holdup structure as well as bubble rise velocities for the two bubble classes. The problems associated with obtaining accurate disengagement profiles were also discussed by Lee et al. (1985), who developed a digital sensor with a computer interface that greatly improved accuracy and reproducibility of the measured disengagement profile.

Researchers at Mobil (Kuo, 1985) were the first to discretize Sriram and Mann's original equation without introducing any new assumptions other than a noncontinuous distribution. They applied the resulting equations to disengagement profiles obtained from experiments using molten wax as the liquid medium at low gas velocities and assumed either unimodal or bimodal bubble size distributions. The quantities estimated in their study included the gas holdup structure, bubble rise velocities, and bubble sizes.

The dynamic gas disengagement technique offers several advantages over the previously mentioned techniques. Bubble size distributions obtained from DGD are based

on the entire dispersion; whereas, all other techniques mentioned above are local measurement techniques. We have shown previously (Bukur et al., 1987a,c and Patel et al., 1990) that the bubble size distribution is a function of radial position (i.e. larger bubbles rise through the center of the column). Thus, when employing any of the "probe" techniques or even photography, measurements must be made at numerous radial positions to obtain an accurate estimate of the Sauter mean bubble diameter. The major drawback with DGD is the fact that bubble sizes are not measured directly.

The purpose of this study was to determine bubble size distributions, and consequently specific gas–liquid interfacial areas for FT–300 wax and SASOL reactor wax in both the 0.05 and 0.21 m ID bubble columns. A description of the DGD technique, the theory associated with DGD, and results from experiments conducted with waxes (FT–300 and SASOL) are presented.

Experimental Techniques for Measurement of the Disengagement Profile

The DGD technique requires an accurate measurement of the rate at which the gas–liquid dispersion drops once the gas flow to the bubble column is shut off. As mentioned previously, one of the problems associated with this technique is determination of the rate at which the liquid level drops during the initial period of disengagement. The majority of previous studies (transparent systems) utilized a video camera/VCR system to measure the rate at which the dispersion dropped once the gas flow was shut off. During large bubble disengagement, the top of the dispersion is not well defined because of splashing caused by the disengagement of large bubbles. In the current study, a video camera/VCR system could not be used since measurements were made in stainless steel columns. Thus, pressure transducers were used to measure the rate at which the liquid level dropped during the disengagement process. The use of pressure transducers not only enables one to use this technique in opaque systems, but also reduces the

subjectivity involved in estimating the rate at which the liquid level drops during large bubble disengagement. In our previous studies (Bukur et al., 1987a,c; Patel et al., 1990), DGD was used to obtain bubble size distributions for a variety of waxes in the 0.05 and 0.23 m ID glass bubble columns. During these studies, the rate at which the liquid level dropped, once the gas flow had been interrupted, was recorded with a video camera/VCR system.

The primary difference in the analysis of data obtained from different forms of data acquisition (i.e. video system vs. pressure transducers) is the frame of reference. Analysis of data obtained from visual observations (i.e. video system) is based on the cross–sectional area of the liquid in the gas/liquid dispersion; whereas, analysis of data obtained from pressure transducers is based on the cross–sectional area of the dispersion. For the former, the volume of liquid in the dispersion remains constant, but the total volume of the dispersion changes (Patel et al., 1989); whereas, for the latter, the total volume of the dispersion below the pressure transducer remains constant but the volume of the liquid varies.

Theory

In the following analysis, we will assume that the dispersion is axially homogeneous and no bubble–bubble interactions occur once the gas flow is interrupted. These are the same assumptions as those used by Sriram and Mann (1977). Deviations from these assumptions may occur in strongly coalescing systems (e.g. air–water system) at high gas flow rates. The assumption of axial homogeneity may also be violated with noncoalescing systems in which there is a high concentration of fine bubbles at the top of the dispersion.

For simplicity, we have assumed a bimodal distribution; however, equations are also presented for multimodal distributions. The dispersion for a bimodal distribution may

be partitioned into three fractions representing the liquid volume, total volume of large bubbles, and total volume of small bubbles. Under the assumption of axial homogeneity, the dispersion, just before gas flow is cut off, may be represented by Figure 5.1. Since information is not obtained for the dispersion above the pressure transducer, no distinction is made between large and small bubbles in this region. The volumes of the three components are proportional to the respective holdup fractions. The disengagement process may be envisioned as either a constant rate process, case I, where the small and large bubbles disengage independent of one another, or as an interactive process, case II, where the disengagement of large bubbles retards the disengagement rate of small bubbles. Even though the latter case is interactive, it does not account for bubble–bubble interaction (i.e. coalescence and breakup). A third, although less likely possibility, is the case where the disengagement rate of small bubbles is enhanced by the disengagement of large bubbles. This could occur if small bubbles adhere to the surface of large bubbles and disengage along with them. The actual disengagement process is expected to lie between the two extremes described above (i.e. case I and case II).

Case I. Constant Rate Disengagement Process

Before analyzing this case, it is important to define the constant rate disengagement process. Under this condition, the volumes representing the large and small bubbles (Figure 5.1) move away from the bottom of the column (disengage) at constant rise velocities. Furthermore, if we assume each volume to be a column of gas with a constant cross sectional area, then this constancy is preserved during the time it takes that column of gas to disengage. At any time during the first period of disengagement (Figure 5.2), the volume of liquid passing below the pressure transducer (V_ℓ) must be the same as the volume of gas associated with the small (V_s) and large (V_L) bubbles which rise above the pressure transducer. Thus, at any time t, a volume balance between the

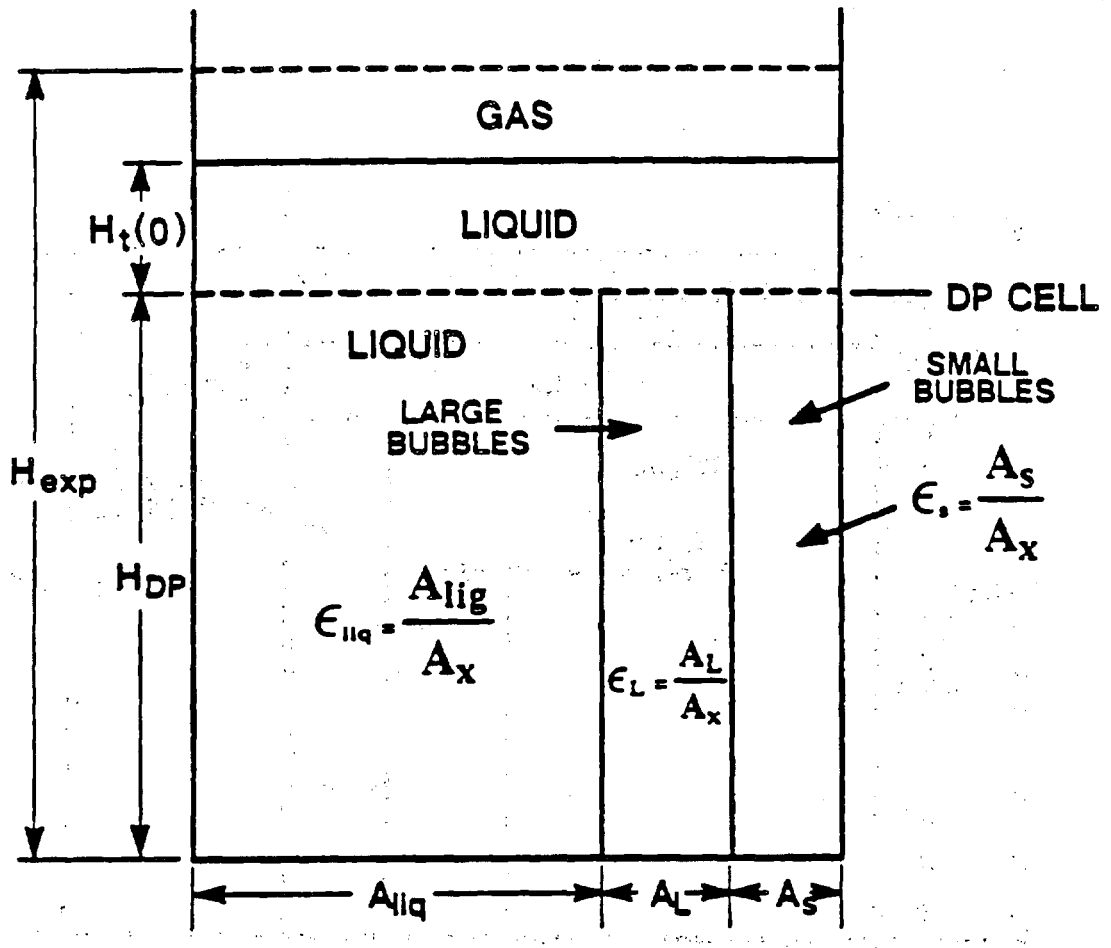

Figure 5.1. Dispersion prior to disengagement (t = 0).

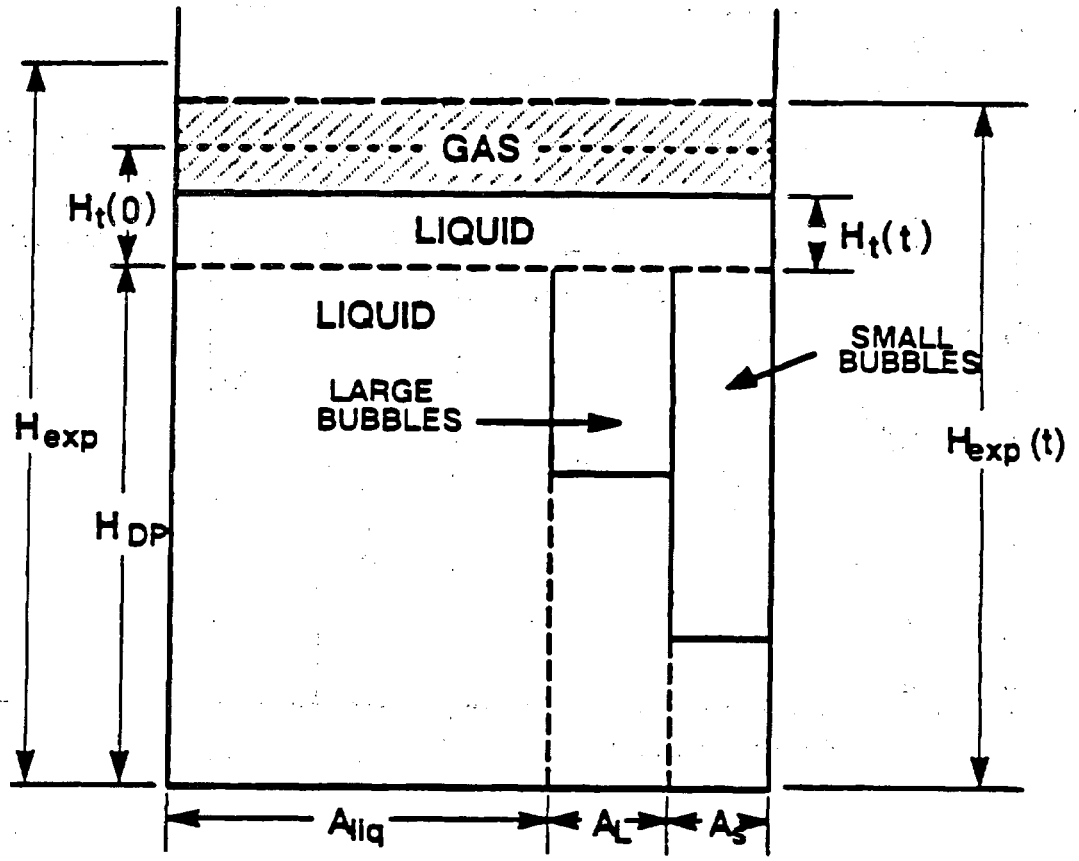

Figure 5.2. Dispersion during the constant rate disengagement process (Period 1).

liquid entering and gas exiting is

$$V_\ell(t) = V_s(t) + V_L(t) \tag{5.2}$$

Furthermore, by the definition of the constant rate disengagement process, the distance between the rear of the small or large bubble swarm would simply be the product of the respective rise velocity and the time elapsed since the initiation of the disengagement process.

The volume of liquid passing below the pressure transducer at any time t may be expressed as

$$V_\ell(t) = V_o - V(t) \tag{5.3}$$

where V_o is the volume of liquid above the pressure transducer immediately prior to interruption of the gas flow and V(t) is the volume of liquid above the pressure transducer during the disengagement process at time t. Substituting Eq. 5.3 into Eq. 5.2 and expressing volumes in terms of heights yields upon rearrangement

$$H_t(t)A_x = H_t(0)A_x - t[u_{bs}A_s + u_{bL}A_L] \tag{5.4}$$

where $H_t(t)$ is the height of liquid above the pressure transducer at time t, $H_t(0)$ is the initial (i.e. at steady state) height of liquid above the pressure transducer, A_x is the cross–sectional area of the column, u_{bs} is the rise velocity of small bubbles, A_s is the cross–sectional area of the column of small bubbles (see Figure 5.1), u_{bL} is the rise velocity of large bubbles, A_L is the cross–sectional area of the column of large bubbles, and t is the time. The cross–sectional area of bubbles of size i (i = s or L) divided by the cross–sectional area of the column represents the volume fraction of gas corresponding to bubbles of size i. Thus, dividing Eq. 5.4 by A_x yields

$$H_t(t) = H_t(0) - t[u_{bs}\epsilon_{gos} + u_{bL}\epsilon_{goL}] \tag{5.5}$$

where ϵ_{gos} is the volume fraction of small bubbles at steady state conditions and ϵ_{goL} is the volume fraction of large bubbles at steady state conditions. The above equation is valid as long as large bubbles are present below the pressure transducer (i.e. for $t < H_{DP}/u_{bL}$, where H_{DP} is the height of the pressure transducer above the distributor).

Similarly, a balance equation for the liquid entering the section of the column below the pressure transducer during the second period of disengagement (Figure 5.3) may be written as

$$V_\ell(t) = H_t(t_1)A_x - H_t(t)A_x = u_{bs}A_s(t - t_1) \qquad t \geq H_{DP}/u_{bL} \tag{5.6}$$

where t_1 corresponds to the time at which all large bubbles passed by the pressure transducer (i.e. $t_1 = H_{DP}/u_{bL}$), $H_t(t)$ is the height of liquid above the pressure transducer at time t and $H_t(t_1)$ is the height of liquid above the pressure transducer at the beginning of period 2 (i.e. small bubble disengagement). Dividing Eq. 5.6 by the cross–sectional area of the column, A_x yields upon rearrangement

$$H_t(t) = H_t(t_1) - u_{bs}\epsilon_{gs}(t - t_1) \qquad t \geq H_{DP}/u_{bL} \tag{5.7}$$

For a multimodal distribution, the following expression is used to describe the rate at which the level drops during the disengagement of bubbles of size j

$$H_t(t) = H_t(t_k) - \sum_{i=j}^{n} u_{bi}\epsilon_{gi}(t - t_k) \qquad k = j - 1, \quad t_k < t < H_{DP}/u_{bj} \tag{5.8}$$

where n is the total number of bubble classes. Note $j = 1$ corresponds to the first period of disengagement and $j = n$ corresponds to the last period of disengagement (i.e. disengagement of the smallest bubbles). Also, for $k = 0$ (i.e. $j = 1$), $t = 0$.

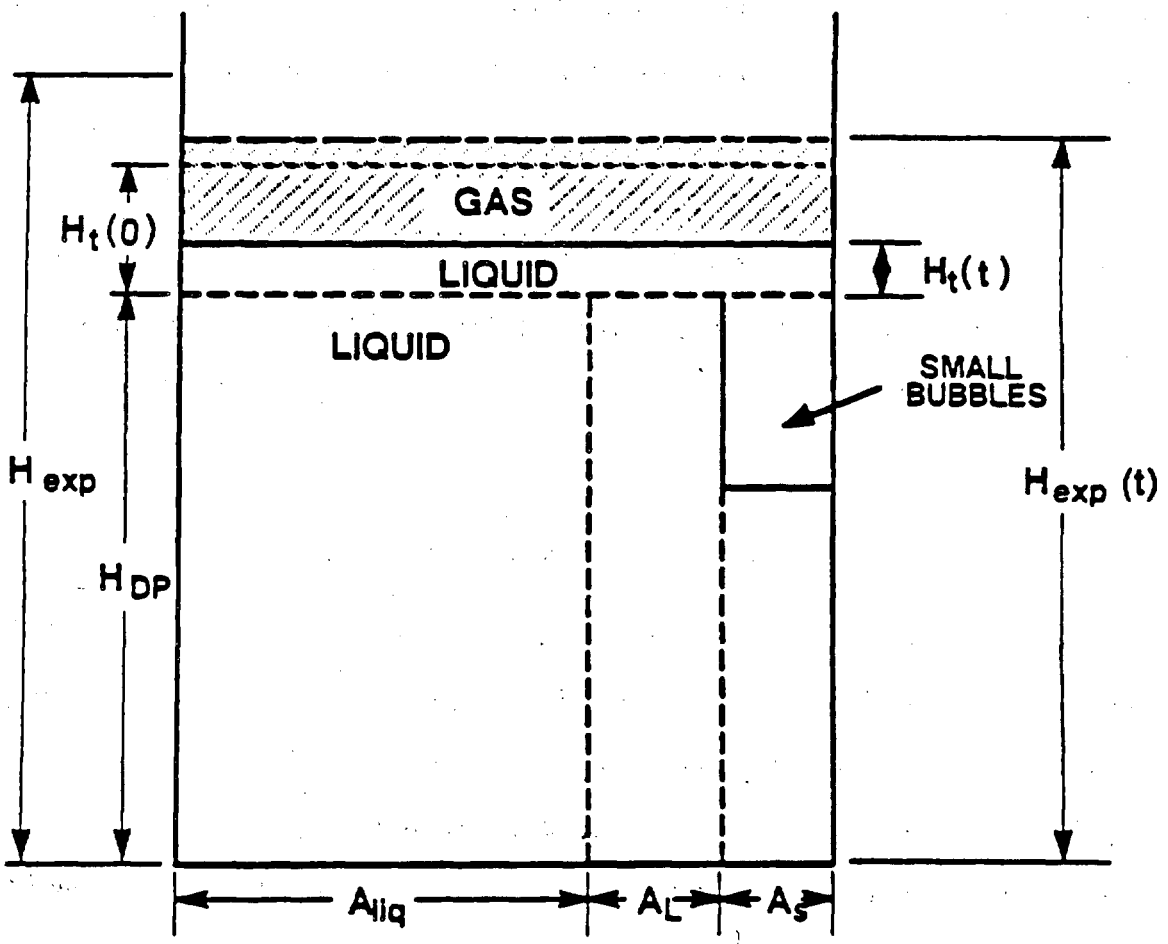

Figure 5.3. Dispersion during the constant rate disengagement process (Period 2).

Estimating Bubble Rise Velocities and Gas Holdups During Constant Rate Disengagement

Equation 5.8 implies that a plot of height of liquid above the pressure transducer, $H_t(t)$, versus time, t, should yield a series of straight lines (Figure 5.4) which may be used to determine the rise velocities and volume fractions of bubbles in the dispersion. Since we assumed that the bubbles disengaged from the bottom of the column at a constant rate, the rise velocity associated with bubbles of size j is simply

$$u_{bj} = \frac{H_{DP}}{t_j} \tag{5.9}$$

where t_j is the time at which the last bubble of size j, passed above the pressure transducer. Once the rise velocities of the bubbles are determined, the gas holdup corresponding to bubbles of size j can be obtained from Eq. 5.8, and is expressed as follows

$$\epsilon_{goj} = \frac{-S_j - \sum_{i=j+1}^{n} u_{bi}\epsilon_{goi}}{u_{bj}} \tag{5.10}$$

where S_j is the slope of the disengagement curve corresponding to the disengagement of bubbles in period j (see Figure 5.4). Eq. 5.10 is solved recursively beginning with j = n (i.e. last period of disengagement). Note, for j=n, $\epsilon_{gon} = -S_n/u_{bn}$.

Estimating Bubble Diameters and the Specific Gas-Liquid Interfacial Area

Bubble rise velocities are estimated from the analysis presented above. However, this analysis does not take into account any radial variations in the rise velocities due to the presence of circulation patterns. This limitation of the DGD technique has been acknowledged in previous studies (e.g. Sriram and Mann, 1977; Schumpe and Grund, 1986), although no effort has been made to introduce any corrective measures. Based on our visual observations using DGD in the glass columns, the dispersion is fairly uniform once all the large bubbles have disengaged. However, during large bubble

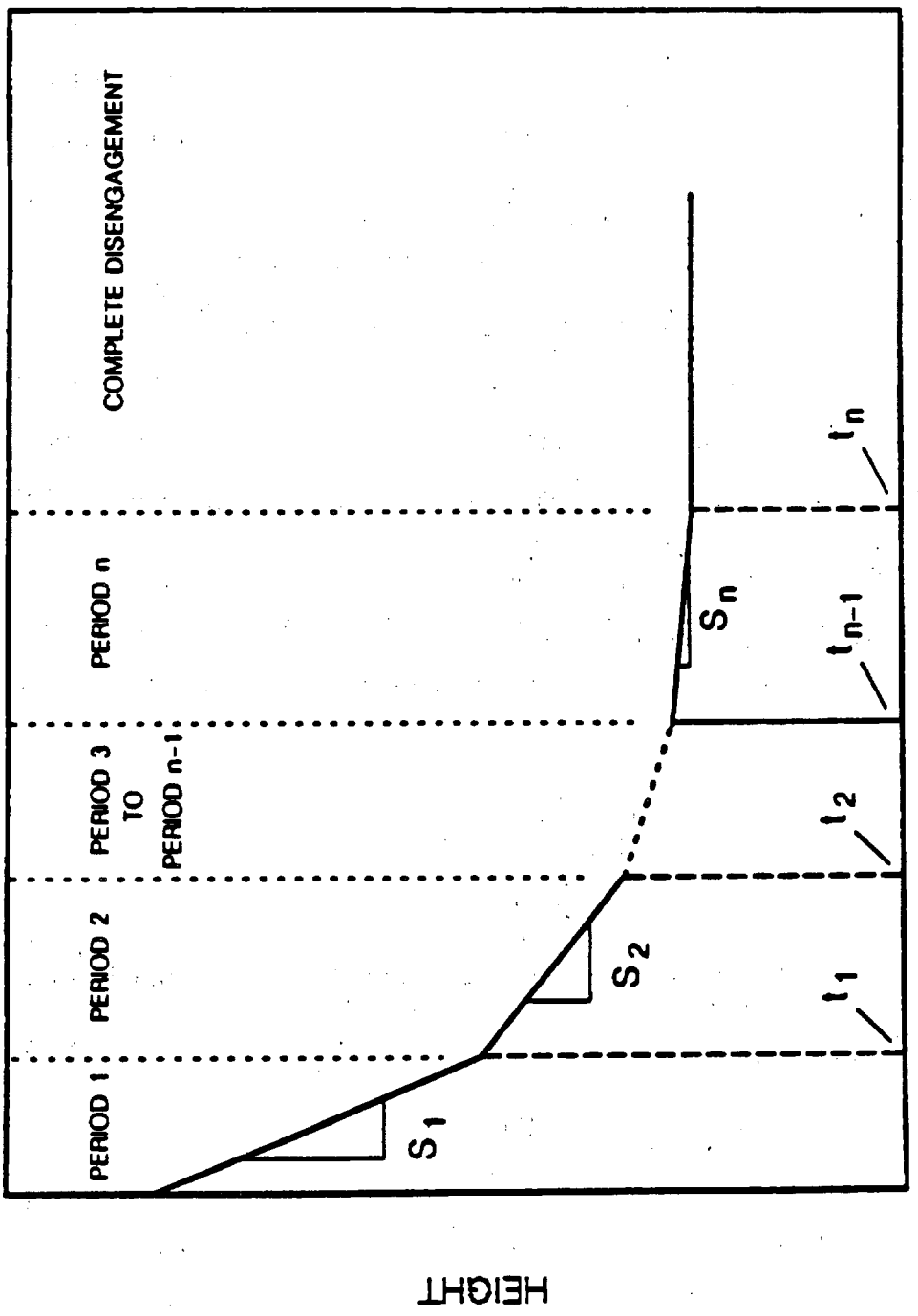

Figure 5.4. Plot of height vs. time for a multimodal distribution (constant rate process).

disengagement, it is possible that strong circulation patterns still exist in the column and the large bubble rise velocities obtained from DGD may not be accurate.

Bubble sizes are estimated from the terminal rise velocity by using appropriate correlations. The correlations used to determine the bubble sizes in the present study are presented in Table 5.1. For the range of rise velocities not covered by these correlations, bubble diameters were obtained by interpolation. Figure 5.5 shows the curve used to determine bubble sizes for FT–300 wax at 265 °C, with the broken line indicating the interpolated region. The correlations by Abou–el–Hassan (1983) and Clift et al. (1978) were used to estimate bubble diameters. The ranges of applicability for these correlations were satisfied for all cases, except for the wax density at 265 °C. At this temperature, the densities of the waxes used in this study (i.e. FT–300 and SASOL) were in the range 660 – 680 kg / m^3, and they are slightly below the range of applicability of the Abou–el–Hassan correlation.

Once the bubble sizes are known, the Sauter mean bubble diameter may be calculated. The definition of the Sauter mean bubble diameter assumes spherical bubbles and is given by

$$d_s = \frac{\sum_{i=1}^{N} n_i d_{Bi}^3}{\sum_{i=1}^{N} n_i d_{Bi}^2} \tag{5.11}$$

where N is the total number of bubble classes, and n_i is total number of bubbles of size d_{Bi}. The number of bubbles of size d_{Bi} may be estimated as follows. The overall gas holdup may be defined as

$$\epsilon_g = \sum_{i=1}^{N} \epsilon_{gi} = \frac{\sum_{i=1}^{N} n_i V_i}{V_t} \tag{5.12}$$

Table 5.1. Correlations for Estimating Bubble Size from Bubble Rise Velocity

Reference	Correlation	Range of applicability
Clift et al. (1978)	$u_b = \left[\frac{2.14\sigma_\ell}{\varrho_\ell d_b} + 0.505 g d_b\right]^{0.5}$	$d_b > 1.3\ mm$
Abou-el-Hassan (1983)	$V = 0.75[log(F)]^2$ $V = velocity\ number = \frac{u_b d_b^{2/3} \varrho_\ell^{2/3}}{\mu_\ell^{1/3} \sigma_\ell^{1/3}}$ $F = flow\ number = \frac{g d_b^{8/3} (\varrho_\ell - \varrho_g) \varrho_\ell^{2/3}}{\mu_\ell^{4/3} \sigma_\ell^{1/3}}$	$710 \le \varrho_\ell \le 1180\ kg/m^3$ $0.233 \le \mu_\ell \le 59\ mPa.s$ $0.015 \le \sigma_\ell \le 0.072\ N/m$ $0.1 \le V \le 40$ $1 \le F \le 10^6$

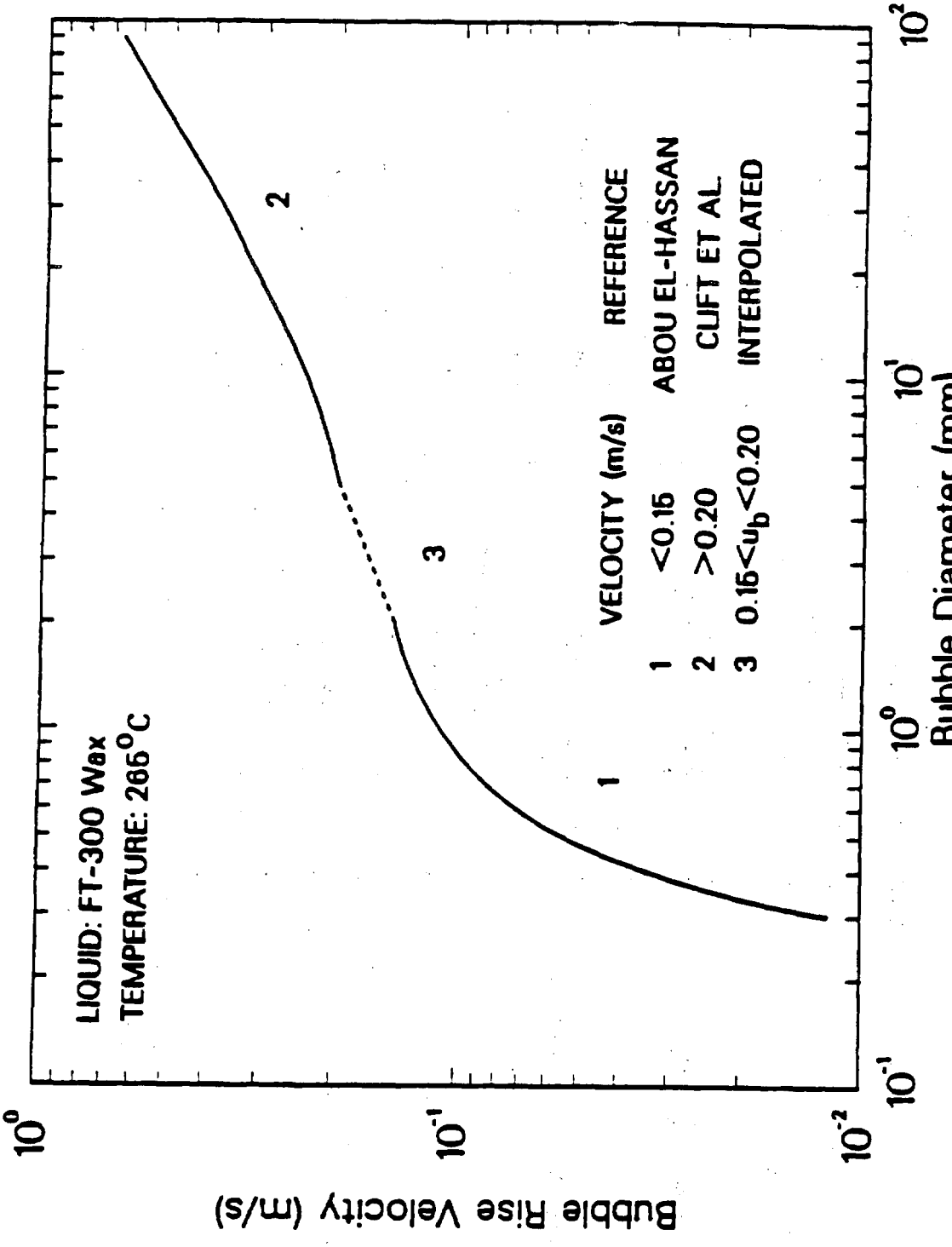

Figure 5.5. Bubble rise velocity vs. bubble diameter correlation for FT-300 wax.

Thus, the number of bubbles in a given bubble class may be written as

$$n_i = \frac{\epsilon_{gi} V_T}{V_i} \tag{5.13}$$

where V_i is the volume corresponding to a bubble of size d_{Bi} and V_T is the total volume of the dispersion below the pressure transducer. Since the volume of an individual bubble is $\pi d_{Bi}^3 / 6$ and the total volume of the dispersion below the pressure transducer is $\pi d_{col}^2 H_{DP} / 4$, Eq. 5.13 may be rewritten as

$$n_i = \frac{3\epsilon_{gi} d_{col}^2 H_{DP}}{2 d_{Bi}^3} \tag{5.14}$$

Substituting the expression for n_i (Eq. 5.14) into the definition of the Sauter mean bubble diameter, Eq. 5.11, the following expression for the Sauter mean bubble diameter is obtained upon rearrangement

$$d_s = \frac{\epsilon_g}{\sum_{i=1}^{N} \epsilon_{gi} / d_{Bi}} \tag{5.15}$$

Data Acquisition and Reduction Procedures

Pressure transducers located at heights of 0.6, 1.3, and 1.9 m above the distributor were used to measure the rate at which the liquid level dropped during the disengagement process. By obtaining data at different heights, knowledge of the axial variation in bubble size distribution may be obtained. After achieving steady state at a given gas velocity ($\approx$ 1.5 hours), the gas flow to the column was shut off using a solenoid valve and the change in the output voltage from the pressure transducer indicators was recorded via the data acquisition system described in Chapter II. Based on our previous work (Bukur et al., 1987a) disengagment was complete within 2 minutes; thus, during the present studies, disengagement data (i.e. output voltages) were acquired for approximately 2 minutes at a sampling frequency of 10 Hz once the gas flow to the

column was terminated. The output voltage from each pressure indicator was converted to pressure (inches of water) using the calibration curves (see Chapter II)

$$\text{P (inches of water)} = \text{SLOPE} * (\text{OUTPUT VOLTAGE}) + \text{INT} \tag{5.16}$$

The pressure, P, may be expressed in "inches of wax" by

$$\text{P (inches of wax)} = \frac{\text{P (inches of water)}}{s_\ell} \tag{5.17}$$

where s_ℓ is the specific gravity of wax. Numerically, the pressure (inches of wax) corresponds to the height of liquid wax above a given pressure transducer.

Typical output voltage versus time data at heights of 0.6, 1.3, and 1.9 m above the distributor from the batch experiment with FT-300 in the 0.05 m ID column at a superficial gas velocity of 0.06 m/s are shown in Figures 5.6a, 5.6b, and 5.6c, respectively. The disengagement profiles at heights of 1.3 and 1.9 m are well defined, but their is a significant amount of oscillations in the disengagement curve acquired at a height of 0.6 m above the distributor. The variation in the disengagement curve at a height of 0.6 m are due to oscillations in the pressure caused by the disengagement of large bubbles from the dispersion. Due to the uncertainty in the disengagement curve at a height of 0.6 m, data obtained at this height were not analyzed.

The original disengagement curve was smoothed by dividing it into 120 equally spaced intervals. This was done by averaging the output voltage for every ten data points, with the exception of the five points at the beginning and end of the disengagement curve. Following this, the slope between successive points were calculated. If successive slopes varied by less than 0.5 %, then the slopes of the two lines were assumed to be the same, and the point common to both lines was omitted, thus reducing the number of bubble classes by one. In general, this reduced the 120 bubble classes to approximately 10 to 20. The output voltage of each data point was then converted to

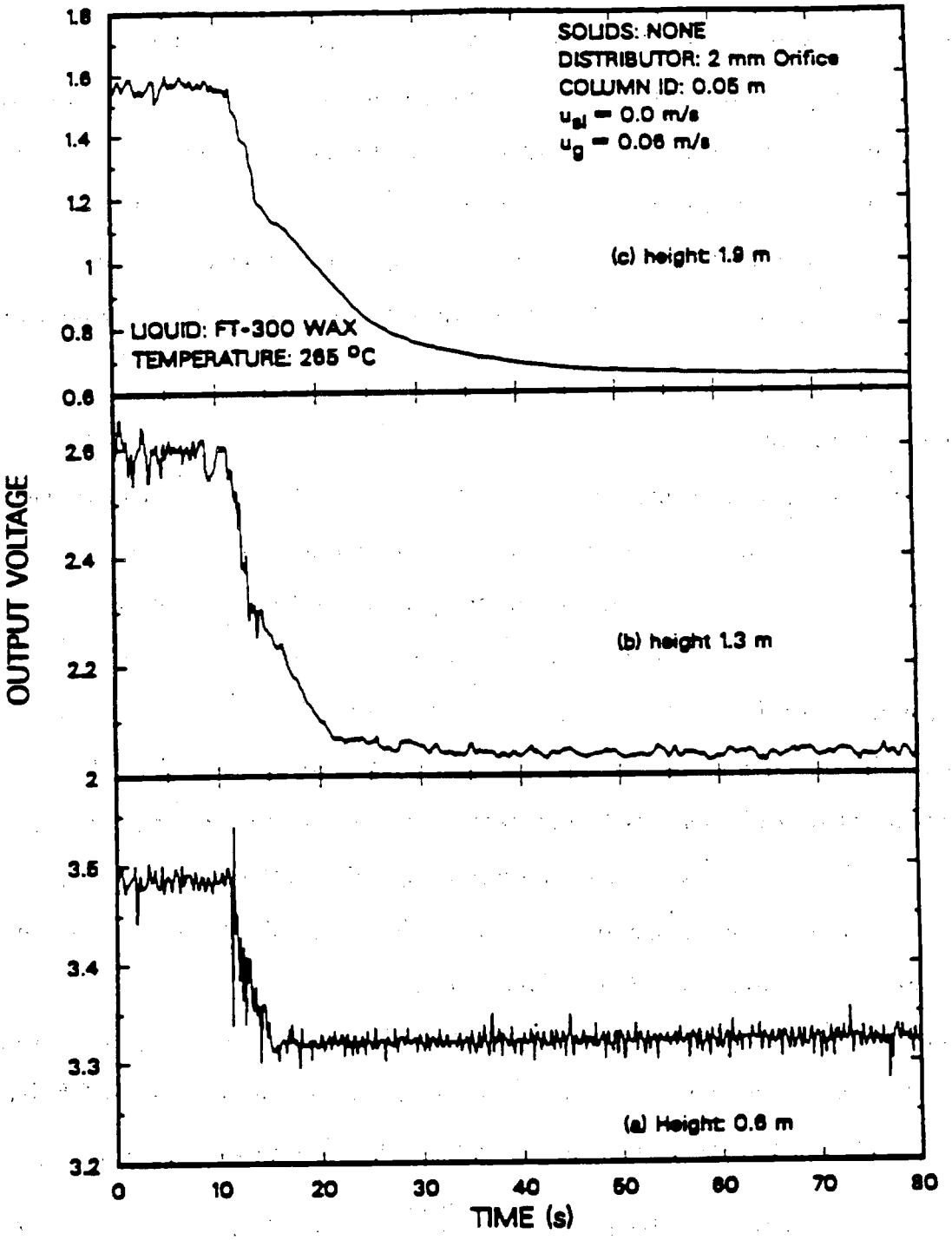

Figure 5.6. Raw pressure transducer signal for DGD analysis from the experiment with FT-300 wax in the small diameter column at heights of (a) 0.6 m; (b) 1.3 m; and (c) 1.9 m above the distributor.